A SIMPLE PREDICTIVE MODEL FOR BENDING OF SHAPE MEMORY POLYMERS

I.T.Garces[1], X. Ma., T.Tang*[2] , and C.Ayranci*[3]

[1] Ottawa, Canada, Carleton University, irinagarces@cunet.carleton.ca
[2] Edmonton, Canada, University of Alberta, ttang@ualberta.ca
[3] Edmonton, Canada, University of Alberta, cayranci@ualberta.ca

Keywords: Shape memory effect, Analytical model, Bending

ABSTRACT

Shape Memory Polymers (SMPs) are versatile materials used in various engineering applications, including self-deployable structures, soft robotics, self-sensing actuators, and biomedical applications. However, the lack of simple and easily applicable predictive models for initial design hampers their potential. Key criteria for conceptual design involve assessing the material's force, speed, and total recovery, which depend on dimensions and loading configurations. While SMPs are commonly subjected to bending in applications like soft robotics and Unmaned Aerial Vehicles (UAVs). Most existing models focus on tension or compression, with some needing to be simplified for practical use. This study presents a straightforward model specifically for bending applications, which serves as a foundation for designing self-actuated 3D printed shape memory polymers and expands the understanding of shape memory polymer composites.

1 INTRODUCTION

Shape Memory Polymers (SMPs) are materials that can be used for many engineering applications, such as self-deployable and self-assemble structures [1] [2], soft robotics [3] [4], self-sensing actuators [5], and in biomedical applications [6]. Although there is a great potential for engineering design with these materials, this is hindered by the lack of simple and easy-to-apply predictive models for first-stage design. Shape morphing materials are increasingly used in human-computer interaction to create interaction mediums. The force that needs to be exerted by the material to achieve mechanical actuation, as well as the speed and degree of recovery, are crucial criteria that need to be assessed for any conceptual design, and it is imperative to predict their dependence on the dimensions and loading configuration. This study is motivated by the lack of models that are of quick application for the engineering design of thermoplastic SMPs.

SMPs are most often subjected to bending, e.g. in soft robotics [4] [7], since this yields the ability to produce large displacements with relatively low applied strains. Many great efforts have been made in accurately modelling SMPs; however, most developed models consider the loading mode to be in tension or compression; others are too complex to allow easy application and interpretation. The present work provides a simple model for bending applications that can approximate the maximum shape recovery force and the shape recovery ratio with respect to time. In this work, we will show the model formulation and the application to a beam under 3-point bending.

In the present work, the authors have applied Tobushi's model [8], derived from a standard linear solid model, to a bending configuration. This model considers an SMP beam under bending deformation. The model has been experimentally validated, and free-end recovery test results are shown in this work. The authors envision a software application that may be provided to designers and engineers to estimate the recovery properties of the material to be used. This application can be populated with a library of different smart materials and their composites.

2 MODEL

This proposed model is based on the viscoelastic model of Tobushi et al. (1997). The constitutive equation for this model is presented in Equation 1, where the strain rate $\dot{\varepsilon}$ can be expressed in terms of the strain, ε, and stress, σ. Additionally, the model compensates for thermal expansion, where α is the coefficient of thermal expansion and $\dot{T}$ is the rate of temperature change. We will ignore the contributions of the coefficient of thermal expansion in the following expression for the sake of simplicity. Still, we understand that this contributes to any inaccuracies in the model. E, μ, and λ are the elastic response of the system, coefficient of viscosity, and retardation time, respectively. These parameters are related to the rheological model in Figure 1 as expressed in Equations 2, 3 and 4, where E_1, E_2, and η are the temperature-dependent rheological parameters.

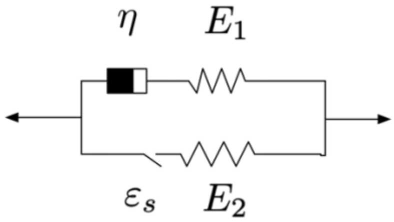

Figure 1: Tobushi's model

$$\dot{\varepsilon} = \frac{\dot{\sigma}}{E} + \frac{\sigma}{\mu} - \frac{\varepsilon - \varepsilon_s}{\lambda} + \alpha\dot{T} \tag{1}$$

$$E(T) = E_1(T) + E_2(T) \tag{2}$$

$$\mu(T) = \frac{\eta(T)E(T)}{E_1(T)} \tag{3}$$

$$\lambda(T) = \frac{\mu(T)}{E_2(T)} \tag{4}$$

The inclusion of the friction element, ε_s, originated from experiments conducted by Tobushi et al. [9]. These experiments involved subjecting the material to a constant load at varying temperatures (creep loading). The results revealed a consistent, temperature-dependent irrecoverable strain during creep, which remained irreversible at the specific temperature [10]. It is important to note, as emphasized by Bhattacharyya et al.[10], that this particular strain during creep should not be confused with plastic strain. Consequently, the friction element ε_s becomes apparent when the creep strain ε_c, defined as the disparity between the total strain and the elastic strain response (as depicted in equation 5), surpasses a threshold value ε_L. This threshold value ε_L is contingent upon temperature, as proposed by Tobushi et al. [21].The model distinguishes three regimes based on the values of creep strain (ε_c) and a temperature-dependent threshold (ε_L). Regime 1 occurs when ε_c is below ε_L, regime 2 when ε_c exceeds ε_L and the strain rate is positive, and regime 3 when the strain rate is negative. The irrecoverable strain (ε_s) depends on the regime, and its expression is shown in equation 7.

$$\varepsilon_c = \varepsilon(t) - \frac{\sigma(t)}{E(T)} \tag{5}$$

$$\varepsilon_s(t,T) = \begin{cases} 0 & \varepsilon_c(t_1) < \varepsilon_L(T) \\ C(T)(\varepsilon_c(t) - \varepsilon_L(T) & \varepsilon_c(t_1) \geq \varepsilon_L(T), \dot{\varepsilon}_c(t_1) > 0 \\ \varepsilon_s(t_1,T) & \dot{\varepsilon}_c(t_1) \leq 0 \end{cases} \tag{6}$$

To simplify the model, effective parameters ($\mu_{eff}, \lambda_{eff}, \varepsilon_{s_{eff}}$) are introduced to cover the three regimes (equation 8), and the notation of $\mu_{EFF}, \lambda_{EFF}, \varepsilon_{s_{EFF}}$ to provide a universal expression for the constitutive relation (equation 9).

$$\dot{\varepsilon}(t>\tau)=\begin{cases}\dfrac{\dot{\sigma}(t)}{E(T)}+\dfrac{\sigma(t)}{\mu(T)}-\dfrac{\varepsilon(t)}{\lambda(T)} & \varepsilon_c(\tau)<\varepsilon_L(T)\\ \dfrac{\dot{\sigma}(t)}{E(T)}+\dfrac{\sigma(t)}{\mu_{eff}(T,C)}-\dfrac{\varepsilon(t)}{\lambda_{eff}(T,C)}+\dfrac{\varepsilon_{s,eff}(T,C)}{\lambda_{eff}(T,C)} & \varepsilon_c(\tau)\geq\varepsilon_L(T),\dot{\varepsilon}_c(\tau)>0\\ \dfrac{\dot{\sigma}(t)}{E(T)}+\dfrac{\sigma(t)}{\mu(T)}-\dfrac{\varepsilon(t)}{\lambda(T)}+\dfrac{\varepsilon_s(\tau,T)}{\lambda(T)} & \dot{\varepsilon}_c(\tau)\leq 0\end{cases} \tag{7}$$

$$\dot{\varepsilon}(\tau<t)=\frac{\dot{\sigma}(t)}{E(T)}+\frac{\sigma(t)}{\mu_{EFF}(T)}-\frac{\varepsilon(t)}{\lambda_{EFF}(T)}+\frac{\epsilon_{s,EFF}(t,T)}{\lambda_{EFF}(T)} \tag{8}$$

The regimes are related to the programming and recovery cycles of the Shape Memory Effect (SME). During programming, the sample is heated to a high temperature (Th) and subjected to a stress (σ). Depending on ε_c and ε_L, the material behaves according to regime 1 or 2. After cooling below the glass transition temperature (Tg), the material enters regime 3. The recovery of the original shape occurs by reheating the material from Tg to Th. In practical applications, the material is often subjected to transient heating that provokes the material to recover before and after the exact temperature Tg; we have also considered this in the model.

3 BENDING MODEL

We have considered a beam that will result in small deformations. The strains along the y-axis are related using Equation 9. This equation incorporates the beam's curvature (κ) and the distance (y) from the neutral axis to a specific point in the y-direction. The material is assumed to exhibit similar behaviour in both compression and tension, leading to the placement of the neutral axis in the middle of the beam's thickness, as depicted in Figure 2. Due to the system's symmetry, analyzing only half of the beam is sufficient. The beam's length is denoted as (L), its height as (H), and its width as (b). By substituting equations 8 and 9 into equation 10, a generalized expression for the moment at any point along the beam can be obtained. The bending moment at each cross-section (*x*) of the beam can be calculated from the stress distribution on the cross-section, and a set of coupled equations can be obtained. The variable (dA) represents the product of beam width (b) and infinitesimal displacement (dy). To evaluate the bending model, a three-point bending test is proposed with a load (P) applied at the center of a simply supported beam (Figure 2).

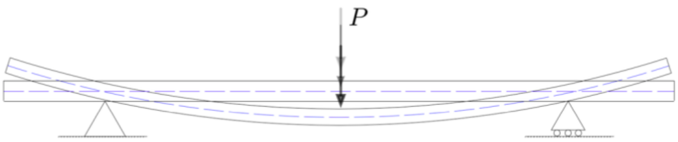

Figure 2: A diagram illustrating the setup of a three-point bending test, showing the neutral axis in blue.

To address the dependence of stress on both (*x*) and (*y*), discretizing the beam is a straightforward approach. Notice that depending on temperature and time, the creep strain (ε_c) may surpass the threshold value ε_L. Consequently, the beam is divided along the y-axis into different regions: regime 1 when $\varepsilon_c < \varepsilon_L$ and regime 2 when $\varepsilon_c \geqslant \varepsilon_L$.

$$\varepsilon=\kappa(t,x)\times y \tag{9}$$

$$M(t,x)\&=\int\sigma(t,x,y)ydA=2\int_0^{H/2}\sigma(t,x,y)bydy \tag{10}$$

4 MATERIALS AND METHODS

4.1 Materials

The experimental validation utilized Shape Memory Polyurethane thermoplastic type (MM7520) obtained from DiAPleX (Tokyo, Japan) in pellet form, (available at www.smptechno.com). This material has a prescribed glass transition temperature (Tg) of 75°C. Injection molding was employed for fabricating all samples using a Sumitomo SE-DUZ machine (Tokyo, Japan). Prior to injection, the material was dried for 24 hours at 100°C using a Lindberg/Blue M oven (Waltham, USA), following the procedures described in previous studies [36]. The samples, with dimensions of 52 mm x 12.7 mm x 3.2 mm, were produced via injection molding and then sanded to achieve flat surfaces.

4.2 Flexural Shape Setting

Flexural bending tests were conducted using an Electroforce BOSE 3200-TA Instruments testing system from New Castle, USA, equipped with a heating chamber. The testing procedure involved raising the chamber temperature to 75°C and stabilizing it for 5 minutes at that temperature. Subsequently, the specimen was subjected to a constant loading rate of $\dot{P}$ =1N/s until reaching a maximum deflection of 5mm at the midspan. Once the maximum deflection was reached and the load was applied, the temperature was lowered to approximately 30°C. Deflection measurements were recorded at a frequency of 10 Hz over time.

4.3 Free end Recovery

Image processing in MATLAB was employed to recognize and track each speckle using a customized code for particle tracking [11]. By utilizing this approach, the displacement of each speckle in the (y) direction relative to the captured frames, as well as any movement tracked in the (x) direction and their trajectories, were determined. To validate the model, colored speckles were drawn onto the sample as to be used as markers. Tracking was focused on the speckle located at the midspan.

4.4 Material Parameter Estimation

Determining material parameters is a crucial and time-consuming task in viscoelastic modelling. It involves extracting values for $\lambda(T)$, $\mu(T)$, and C(T) through extensive testing and analysis of experimental data. Various tests like creep and stress relaxation tests have been used in the past to approximate these parameters. Dynamic Mechanical Analysis (DMA) tests offer a convenient way to obtain the static and dynamic behaviour of the material, represented by the storage modulus (E_s), loss modulus (E_l), and phase angle (δ) between them.

A series of cyclic frequency sweep dynamic mechanical analysis (DMA) tests were performed at various isothermal temperatures. The frequency range for the tests was from 0 to 50 Hz, and the temperatures ranged from 55°C to 80°C in 5°C increments. Different amplitudes were employed during the tests to ensure that the material experienced different levels of strain. Specifically, amplitudes of 15µm, 150µm, 200µm, and 350µm were utilized.

Bhattacharyya et al. [10] proposed an analytical solution for obtaining E_s and $Tan\ \delta$ through periodic strain applied in an SMP model. It should be noted that in this study, the material properties are assumed to be primarily influenced by temperature changes. The adjusted material parameter functions can be observed in Table 1.

Material Parameter	Equation fit	Coefficients
$E(T)$	$\frac{E_\infty e^{-a_e*Tg}+E_o*e^{-a_e*T}}{e^{-a_e*Tg}+e^{-a_e*T}}$	$ae=0.2355; E_\infty=0; E_o=2026$
$\lambda(T)$	$a_l e^{-\left(\frac{T-bl}{cl}\right)^2}+dl$	$a_l=5.511; bl=77.27; cl=3.344; dl=1$
$\mu(T)$	$a_u e^{-\left(\frac{T-bu}{cu}\right)^2}+du$	$a_u=1128; bu=65.5; cu=8.034; du=0$
$C(T)$	$a_c e^{-bcT}$	$a_c=39.81; bc=0.06754$
$\varepsilon_l(T)$	$\frac{\varepsilon l_\infty e^{-a_p*Tg}+\varepsilon l_o*e^{-a_p*T}}{e^{-a_p*Tg}+e^{-a_p*T}}$	$a_p=0.4; \varepsilon l_0=0.0001; \varepsilon l_\infty=0.002$

Table 1: Material parameters adjusted to DMA of SMPs

5 RESULTS

5.1 Shape Setting

Shape setting or shape programming of the material is performed at a constant temperature. The values of the material parameters, such as E_g, μ_g, and λ_g, are directly obtained from the DMA fit at 75ºC. Experimental data for the applied force and displacement during shape setting are shown in Figure 3. A comparison between the predicted and experimental results, represented by the coefficient of determination (R^2), is shown in the figure. The model successfully captures the behaviour of the beam during the shape setting, although there are discrepancies in the maximum deflection between the model and experiments. The best prediction for the specific experimental data is achieved with λ_g=2.6 s. The material parameter ε_l(T) is determined from the programming stage. An optimization process was conducted to minimize the discrepancy between the model and experimental values for the maximum deflection. The value of ε_l(Tg) is obtained as approximately ε_l=0.015.

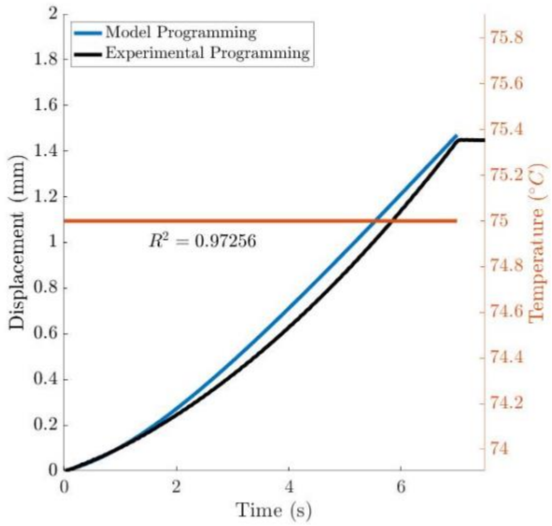

Figure 3: A representative result of the programming step and its prediction.

5.2 Free End Recovery

To normalize the data, the recovery ratio was used, defined as the ratio between the initial deflection at the midspan and the deflection over time with respect to the initial position at the midspan. Experimental results for all heating rates showed high sample deviation but a consistent trend in recovery rate. The model, using material parameters extracted from DMA, predicted faster recovery than observed in experiments. The model failed to predict the irrecovery ratio accurately with the same material parameters, which highlights the need to tune our material parameter extraction or improve the expression for irrecoverable strain evolution. Varying the material parameter λ_0 significantly affected the recovery rate, with higher λ_0 values leading to improved recovery approximation. A comparison between the model (with λ_0 = 35s) and experimental values was presented in Figure 4.

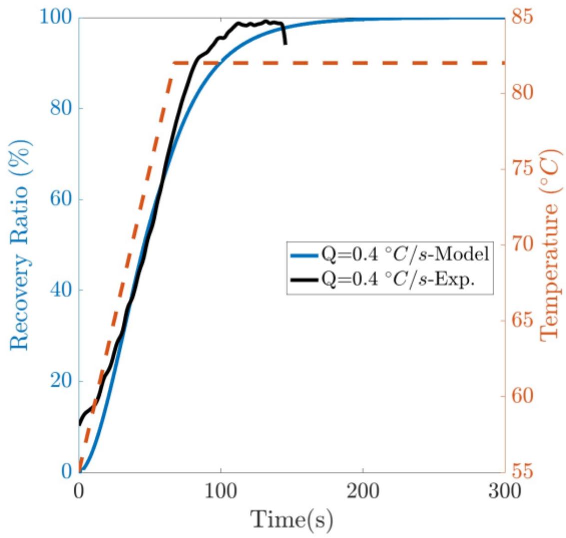

Figure 4: A representative result of the programming step and its prediction.

6 DISCUSSION

The present model aims to capture the transient recovery behaviour of shape memory polymers in bending applications. It is based on Tobushi et al.'s model but has been modified to account for strain variation along the y-axis in a thin beam under small deformations. A DMA procedure has been proposed to extract material parameters, which is typically done through time-consuming tests.

Results for the programming stage and recovery have been presented using the extracted parameters. In this model, we have found a few discrepancies. Possible causes for the discrepancy can be rooted in some of the material behaviour we have assumed. For instance, we have accounted the material's behaviour in compression and tension to be the same, placing the neutral axis in the middle of the beam. This is certainly not necessarily the case as we understand the microstructure changes during tension or compression occur, and especially on a semi-crystalline polymer, these can have significant effects. We have also included the assumption of constant curvature during constrained recovery, which limits how the material will recover in the model. We have ignored energy loss due to internal friction and the contribution of the coefficient of thermal expansion. Further, we know that there is the potential strain-dependent nature of parameters and microstructural changes during cooling due to crystallinity that will immensely affect how the material behaves. The cooling process and its effects on material properties should be investigated further.

7 CONCLUSIONS AND RECOMMENDATIONS

Despite the model's discrepancy, it captures the overall trend of shape recovery force and ratio. This work is followed by a thorough journal publication which details the DMA material parameter estimation, the recovery force and the ratio with respect to a variety of heating rates. Further recommendations for future work include testing at different strains, microstructural analysis, improved parameter expressions, and additional tests at higher amplitudes and different strain levels. Due to the model's straightforward formulation, There is an enormous potential for this model to characterize more advanced and novel structures, such as 3D-printed SMP actuators and sensors. This current model is a stepping stone towards the design of self-actuated 3D printed shape memory polymers and further into shape memory polymer composites.

ACKNOWLEDGEMENTS

The authors would like to acknowledge NSERC Discovery Grant (Ayranci) for the funds supporting this work.

REFERENCES

[1] L. Santo, F. Quadrini, A. Accettura and W. Villadei, "Shape Memory Composites for Self-deployable Structures in Aerospace Applications," *Procedia Engineering*, vol. 88, pp. 42--47, 2014.

[2] A. Todoroki, K. Kumagai and R. Matsuzaki, "Self-deployable Space Structure using Partially Flexible CFRP with SMA Wires," *Journal of Intelligent Material Systems and Structures*, vol. 20, no. 12, pp. 1415--1424, June 2009.

[3] P. Boyraz, G. Runge and A. Raatz, "An Overview of Novel Actuators for Soft Robotics," *Actuators*, vol. 7, no. 3, p. 48, September 2018.

[4] J. Z. Gul, M. Sajid, M. M. Rehman, G. U. Siddiqui, I. Shah, K.-H. Kim, J.-W. Lee and K. H. Choi, "3D printing for soft robotics - a review.," *Science and Technology of Advanced Materials*, vol. 19, no. 1, pp. 243--262, 2018.

[5] I. T. Garces and C. Ayranci, "Active control of 4D prints: Towards 4D printed reliable actuators and sensors," *Sensors and Actuators, A: Physical*, vol. 301, p. 111717, January 2020.

[6] H.-M. Chen, L. Wang and S.-B. Zhou, "Recent Progress in Shape Memory Polymers for Biomedical Applications," *Chinese Journal of Polymer Science (English Edition)*, vol. 36, no. 8, pp. 905--917, August 2018.

[7] S. Barbarino, O. Bilgen, R. M. Ajaj, M. I. Friswell and D. J. Inman, "A review of morphing aircraft," *Journal of Intelligent Material Systems and Structures*, vol. 22, no. 9, pp. 823--877, June 2011.

[8] H. Tobushi, T. Hashimoto, S. Hayashi and E. Yamada, "Thermomechanical constitutive modeling in shape memory polymer of polyurethane series," *Journal of Intelligent Material Systems and Structures*, vol. 8, no. 8, pp. 711--718, January 1997.

[9] H. Tobushi, T. Hashimoto, S. Hayashi, E. Yamada, Thermomechanical constitutive modeling in shape memory polymer of polyurethane series, Journal of Intelligent Material Systems and Structures 8 (8) (1997) 711– 718.

[10] A. Bhattacharyya, H. Tobushi, "Analysis of the isothermal mechanical re- sponse of a shape memory polymer rheological model", *Polymer Engineering &* Science 40 (12) (2000) 2498–2510.

[11] M. Pastor, Simple particle tracking, matlab central file exchange. URL https://www.mathworks.com/matlabcentral/fileexchange/13840-simple-particle-tracking